THE DESIGN OF AC PERMANENT MAGNET MOTORS FOR ELECTRIC VEHICLES: A COMPUTATIONALLY EFFICIENT MODEL OF THE OPERATIONAL ENVELOPE

J.Goss*†, P.H.Mellor*, R.Wrobel*, D.A.Staton†, M.Popescu†

**University of Bristol, UK {R.Wrobel, P.H.Mellor}@bristol.ac.uk †Motor Design Ltd, UK {James.Goss, Dave.Staton, Mircea.Popescu}@motor-design.com*

Keywords: AC PM motor, Operation characteristics, Efficiency, Torque/Speed, Field Weakening

Abstract

Salient brushless AC (BLAC) permanent magnet (PM) motors are a preferred topology in the rapidly growing area of electric vehicle traction due to their inherent high efficiencies and excellent power densities. In the design of these systems it is important to appraise the motor performance across the entire torque-speed envelope. This paper presents computationally efficient techniques that allow rapid and accurate modelling of the entire operational envelope of any BLAC PM motor, enabling the generation of torque/speed characteristics and loss maps that can be used in an iterative design process. The proposed techniques are validated against test data from an in-house 35kW interior PM motor design and a comparison between a measured and computed efficiency map for the 2004 Toyota Prius motor is undertaken.

1 Introduction

The design of BLAC PM motors for traction applications requires consideration of performance across the entire operational envelope that commonly includes a field weakening region. However the optimisation of a design over this performance envelope can be challenging as all currently available computer aided design (CAD) tools only provide analysis of performance at individual operating points.

This paper proposes a computationally efficient technique that enables rapid and accurate evaluation of performance over the entire operating envelope. The method allows the design engineer to generate torque/speed characteristics as well as efficiency and loss maps which can be effectively incorporated into an iterative design process. The proposed approach is based on the classical d-q phasor model, shown in fig. 1, combined with simple polynomial expressions for flux linkage and loss. The required parameters for the analysis are obtained from a reduced set of 2D finite element (FE) field solutions. These are used to account for the non-linearity of the direct and quadrature axis flux linkages caused by saturation and cross coupling effects, and to enable efficient and accurate loss modelling [4].

Torque-speed characteristics and efficiency maps generated by the proposed approach are validated against the data provided in [1] for the 2004 Toyota Prius motor and measurements taken from an in-house 35kW prototype motor.

2 Definition of Motor Operating Point

The established torque and voltage equations for a salient pole AC PM motor are described in (1) and (2). In defining the motor operating point it is sufficient to consider fundamental ac quantities only.

$$T = \frac{m}{2} p(\lambda_m I_q + I_q I_d (L_d - L_q)) \qquad (1)$$

$$V = \omega_s \sqrt{(\lambda_m + L_d I_d)^2 + (L_q I_q)^2} \qquad (2)$$

where T is the torque, m the number of phases, p the number of pole pairs, $I_{d,q}$ the direct and quadrature components of the peak phase current, V is the peak phase voltage, ω_s is the, electrical rotational speed, $L_{d,q}$ is the direct and quadrature axis inductances and λ_m the permanent magnet flux linkage.

In a non-salient machine $L_d = L_q$ whereas for salient PM rotors $L_d < L_q$.

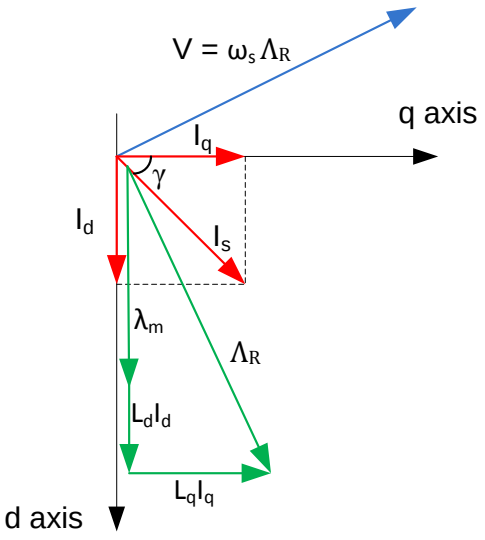

Figure 1: Phasor diagram for a salient PM BLAC motor

In fig.1 Λ_R is the resultant stator winding flux linkage, I_s the magnitude of the peak stator phase current and γ the current advance angle.

The torque/power characteristic of a motor under a given maximum current, I_{smax}, and inverter voltage is shown in fig. 2. The supply current and voltage constraints give rise to the three operating modes shown. When discussing these it is often more intuitive to describe the current in terms of the peak phase current magnitude I_s and advance angle γ, where I_d=-$I_s$sinγ, I_q=$I_s$cosγ.

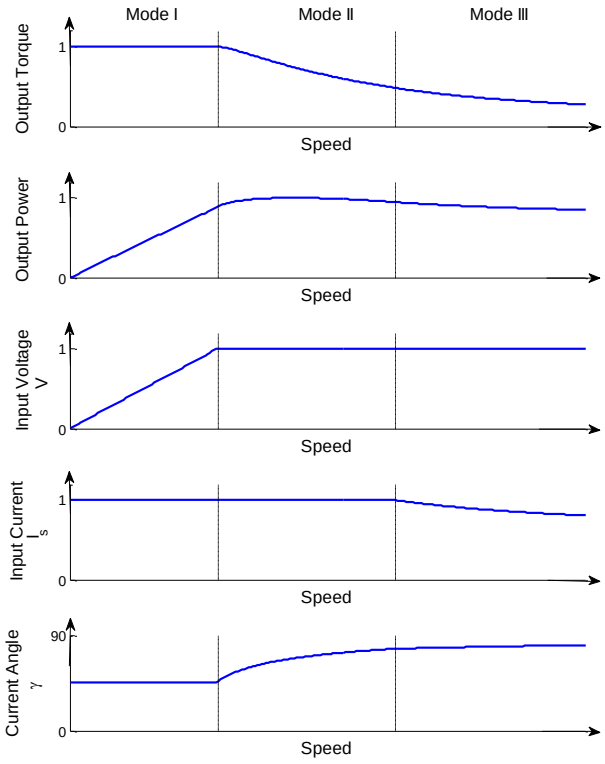

Figure 2: Field weakening behaviour of a BLAC PM motor [7]

Mode I: Current Limited Region, Zero to Base Speed: Here it is desirable to operate with the current angle γ that maximises the torque output for a given current. For a machine with saliency this will occur at a non-zero value of γ due to the reluctance torque component. The input voltage rises linearly with speed.

Mode II: Voltage and Current Limited Region. As the speed is increased the inverter reaches maximum modulation depth, to progress beyond the base speed, the current angle γ is further advanced resulting in a larger magnitude of negative d-axis current which acts to demagnetise the field. This reduces both the d and q axis flux linkages and allows a higher rotational speed for the same voltage however consequently the torque is reduced. In this mode maximum torque is achieved by operating with maximum current I_{smax} and the minimum value of γ that enables operation at the required speed within the given voltage limit.

Mode III: Voltage Limited Region[1]. As the speed is increased further, optimal operation may be achieved with $I_s < I_{smax}$. Hence in this region maximum torque/amp occurs with the value of current and current angle that maximises the torque within the voltage limit.

Since this behaviour is not always intuitive it can be difficult to anticipate the impact of design changes on the operational envelope of the motor.

3 Overview of the Modelling Approach

3.1 Maximum Torque/Amp Operating Point Computation

The maximum torque operating point at any given speed and maximum current magnitude can be described by the optimisation problem characterised by (3)-(5).

Maximise:

$$T = \frac{m}{2} p(\Lambda_d I_q - \Lambda_q I_d) \quad (3)$$

where:

$$V_{lim} \geq \omega_s \sqrt{\Lambda_d^2 + \Lambda_q^2} \quad (4)$$

and:

$$I_{smax} \geq \sqrt{I_d^2 + I_q^2} \quad (5)$$

Here V_{lim} is the maximum voltage available from the inverter and $\Lambda_{d,q}$ are the direct and quadrature axis flux linkages.

For the common linear approximation:

$$\Lambda_q(I_q) = L_q I_q \quad (6)$$

$$\Lambda_d(I_d) = \lambda_m + L_d I_d \quad (7)$$

The parameters of a particular motor design λ_m, L_d and L_q can be obtained beforehand from electromagnetic finite element (FE) analysis or analytical techniques. Using these parameters alongside the specified rotational speed, maximum voltage and maximum current the problem can be solved using a constrained non-linear optimisation algorithm. Values of I_d and I_q that maximise (3) while remaining within the constraints described by (4) and (5) are returned, allowing the torque envelope to be defined over increasing rotational speed steps. The prior definition of the key motor parameters means that the torque speed envelope can be generated in a computationally efficient manner.

Figs 3 and 4 plot the computed output from the algorithm described for an interior permanent magnet (IPM) motor design for a small electric vehicle. The three modes of

[1] Mode III will exist where I_{smax} is greater than the current required to fully demagnetise the field from the permanent magnet if all the current is in the d axis.

operation described in Section 2 are evident in fig. 4. In Mode I only the maximum current constraint, (5), is enforced, in Mode II both the maximum current and maximum voltage constraints, (4) and (5) are active. Finally in Mode III only the voltage constraint, (4), is enforced.

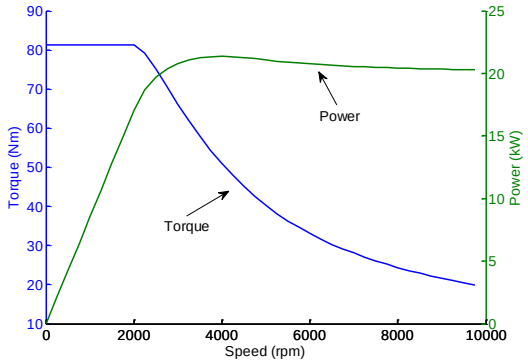

Figure 3: Calculated torque and power speed characteristics

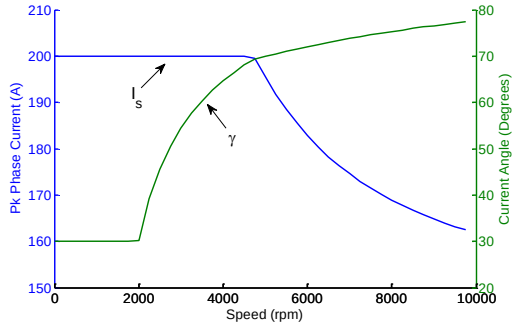

Figure 4: Calculated optimum I_s and γ with increasing speed

3.2 Accounting for Saturation and Cross Coupling

The linear inductance approximation used in (6) and (7) to describe the flux linkage components Λ_d and Λ_q does not account for the effects of cross coupling and saturation [2]. As such this approximation may not be fit for purpose when modelling at high operating current or in the field weakening region [6]. An example of the saturation and cross coupling effects are shown in figs. 5 and 6 where, for a particular motor design, the value of the flux linkages Λ_d and Λ_q have been analysed over a range of different values of direct- and quadrature-axis currents, I_d and I_q through 2D FE calculations.

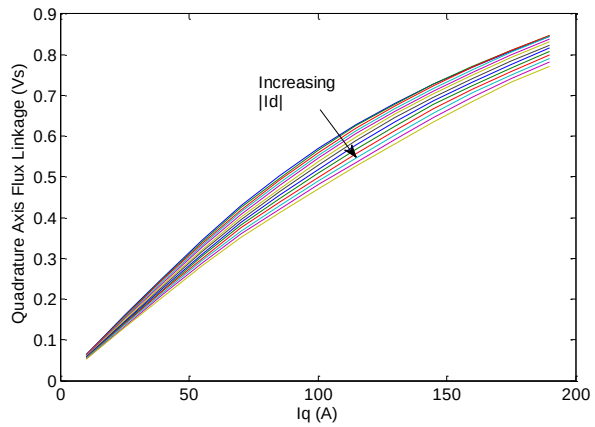

Figure 5: Example variation of Λ_q with I_q and I_d

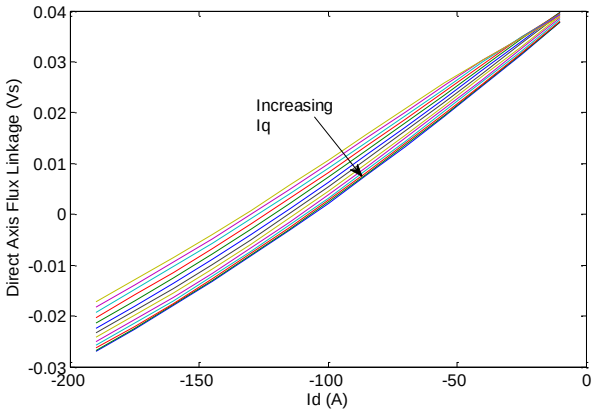

Figure 6: Example variation of Λ_d with I_d and I_q

The variation of Λ_d and Λ_q with both components of current is accurately described by second order polynomial functions, given in (8) and (9) respectively.

$$\Lambda_q(I_d, I_q) = a_q + b_q I_d + c_q I_q + d_q I_d I_q + e_q I_d^2 I_q^2 + f_q I_q^2 + g_q I_d^2 I_q + h_q I_d I_q^2 + j_q I_q^3 + k_q I_d^2 I_q^2 + l_q I_d I_q^3 + m_q I_q^4 \quad (8)$$

$$\Lambda_d(I_d, I_q) = a_d + b_d I_d + c_d I_q + d_d I_d I_q + e_d I_d^2 + f_d I_q^2 + g_d I_d^2 I_q + h_d I_d I_q^2 + j_d I_q^3 + k_d I_d^2 I_q^2 + l_d I_d I_q^3 + m_d I_q^4 \quad (9)$$

A computation comprising 15 2D FE solutions which contain 5 distinct values of I_q and 3 distinct values of I_d provides sufficient data to calculate the coefficients for (8) and (9) using a least squares fitting method. This approach gives high accuracy while keeping the computation time to a minimum.

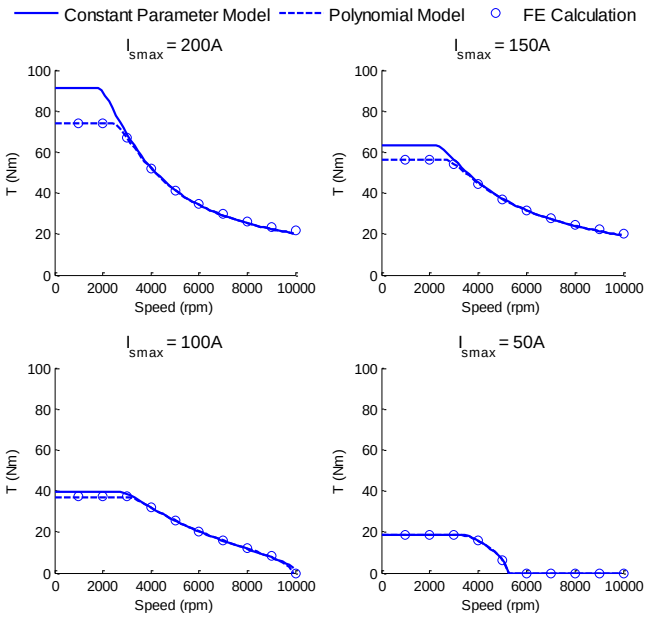

Figure 7: Comparison of torque/speed plots calculated using the constant parameter and flux linkage model

Fig. 7 compares the torque calculated using the linear inductance model described by (6) and (7), using the proposed polynomial fit in (8) and (9) to obtain the flux linkages and a finite element calculation completed at several operating points. As can be seen the proposed polynomial model accurately predicts the torque at all operating points. Whereas the constant inductance model is only accurate in the absence of saturation at low values of currents or during field weakening.

3.3 Iron Loss Modelling

A powerful tool to aid the design process is the rapid creation of efficiency and loss map plots. Accurate computation of iron losses at a single operating point requires a time-stepping FE analysis that can be fairly computationally intensive. Clearly when calculating a large number of operating points it is inappropriate to undertake this computation on each occasion.

In [4] a computationally efficient iron loss model is described that provides accurate iron loss prediction at any operating point from only two time-stepping FE iron loss calculations; at short circuit and at open circuit conditions. The method is expanded here applying the model to a salient PM machine and integrating it with the other techniques developed in this paper.

To create this model in the absence of a circuit coupled FE solver the short circuit current, $I_{sc,}$ needs to be calculated. This is the value of I_s that, at full advance angle (γ= 90°), causes the d axis flux linkage and hence voltage at any rotational speed to be zero. Given $I_q=0$ at short circuit, I_{sc}, can be found from the earlier d-axis flux linkage mapping (9):

$$I_{sc} = \frac{b_d \pm \sqrt{{b_d}^2 - 4e_d a_d}}{2e_d} \qquad (10)$$

Time-stepping FE analyses are then performed at a single nominal frequency, f, to find the total iron loss at open circuit, $I_d=0$ $I_q=0$, and short circuit, I_d= -I_{sc} $I_q=0$. Using the two term version of the modified Steinmetz equation equivalent hysteresis and eddy current coefficients a_h, a_e, b_h, b_e are returned as indicated in (11) and (12).

$$P_{FE}^{OC}(f) = a_h f + a_e f^2 \qquad (11)$$

$$P_{FE}^{SC}(f) = b_h f + b_e f^2 \qquad (12)$$

The total iron loss is separated into two components, g_1 and g_2, given in (14) and (15), induced by the main magnetising flux path and demagnetising flux path respectively. The strength of these flux paths can be approximated by $V_{m,}$ the magnetising voltage and V_d^* the demagnetising voltage, (16) and (17). In (13), (14) the permanent magnet component of the flux linkage is from $\Lambda_d(I_d,I_q)$, (8) with $I_d = 0$, (15).

$$g_1(V_m) = \frac{a_h}{2\pi\lambda_m(I_q)} V_m + \frac{a_e}{2\pi\lambda_m(I_q)^2} {V_m}^2 \qquad (13)$$

$$g_2(V_d^*) = \frac{b_h}{2\pi\lambda_m(I_q)} V_d^* + \frac{b_e}{2\pi\lambda_m(I_q)^2} {V_d^*}^2 \qquad (14)$$

$$\lambda_m(I_q) = \Lambda_d(0, I_q) \qquad (15)$$

where

$$V_d^* = -2\pi f(\Lambda_d(I_d, I_q) - \lambda_m(I_q)) \qquad (16)$$

and

$$V_m = 2\pi f \sqrt{\Lambda_d(I_d, I_q)^2 + \Lambda_q(I_d, I_q)^2} \qquad (17)$$

The total iron loss can then be calculated at any operating point from the sum of $g_1(V_m)$ and $g_2({V_d}^*)$ as shown in (18).

$$W_{fe} = g_1(V_m) + g_2(V_d^*) \qquad (18)$$

Fig. 8 compares the calculated iron losses using the above voltage model with the iron loss obtained from separate FE simulations for a set value of maximum current and over a full speed range for a salient IPM traction motor design. Good agreement is obtained, with the voltage model slightly overestimating the loss.

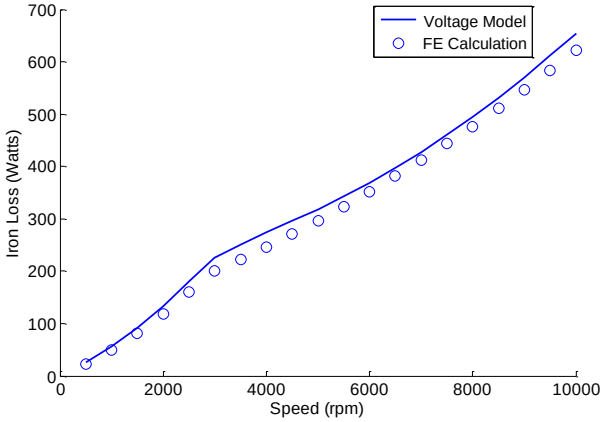

Figure 8: Comparison of voltage model with FE calculations

4 Experimental Validation

The torque envelope computation and flux linkage model described in Sections (3.1) and (3.2) have been validated against an in-house water jacket cooled, 30 slot, 8 pole, 35kW IPM traction motor design. For this motor a set of measurements were taken at a low speed with a fixed value for the stator current, I_s and the current angle was advanced in 10° increments from 0° to 90°, with each measurement recorded at thermal steady state. The results were repeated at 25A_{rms} steps up to a maximum of 200A_{rms}.

At each test current a curve fit was used to find the maximum torque, $T_{meas,}$ and current angle to achieve this torque, γ_{meas}, Table I. The maximum torque/amp is achieved at a non-zero

value of γ due to the reluctance torque component that arises from the machine's saliency.

The corresponding values of torque and current angle, T_{fe} and γ_{fe}, are obtained from an FE model of the motor using a similar approach to the measured data. The value of I_s is set and γ is incremented in small steps resulting in numerous FE calculations. For this analysis a commercial FE design tool [5] is used. The optimal operating point shown in Table I is then found by plotting the generated torque versus current angle data and taking the maximum of the curve.

Finally the optimal torque and current angles, T_{model} and γ_{model}, are computed using the method described in Section 3. The coefficients used in the polynomial expressions for flux linkage, (8) and (9) are given in the Appendix.

I_{rms}(A)	T_{meas} (Nm)	γ_{meas} (˚)	T_{fe} (Nm)	γ_{fe} (˚)	T_{model} (Nm)	γ_{model} (˚)
24	15	7	15	7	15	8
50	32	14	32	13	31	14
75	48	16	49	17	49	17
100	66	20	66	20	66	19
124	83	22	83	22	83	22
150	100	24	101	24	101	24
175	117	26	119	25	119	25
200	134	27	136	27	136	26

Table I: Validation of operating point and electromagnetic torque calculation

There is good agreement between all three data sets. The method proposed in Section 3 is far more computationally efficient than a complete mapping of the torque versus current angle space through individual FE analyses and is therefore a valuable approach for the rapid computation of the maximum torque per amp operating point. It should be noted there is a slight over prediction of the torque at the higher values of I_s against the measured data. This is due to the models assuming a consistent temperature across all operating points. Since each measured data point is taken at thermal steady state the higher current measurements correspond to higher operating temperatures; the permanent magnet flux reduces with increased magnet temperature hence the slight over-prediction of the torque.

The proposed techniques have also been applied to model the operational envelope of a 2004 Toyota Prius motor for which a comprehensive set of test data and corresponding efficiency map is given in [1]. An efficiency map generated from this test data is shown in fig. 9; an efficiency map computed using the proposed methods compares well and is shown in fig. 10. The total computation time for generating this data on a PC with a 2.83GHz processor and 8GB of RAM is approximately 3½ minutes. A breakdown of the computation times is shown in Table II.

In the efficiency calculations a build factor of 2.2 has been used with the iron loss calculations to account for any degradation in the material properties during the stamping and assembly of the lamination stack. A per phase resistance of 9.3mΩ has been calculated from the slot area and copper fill factor. The mechanical loss is taken from [3] in which a measured loss of 2.4kW at 6000rpm for the Prius motor with a dummy rotor is given. Magnet loss and AC copper loss effects are neglected. The computed coefficients for the flux linkage and iron loss equations are given in the Appendix.

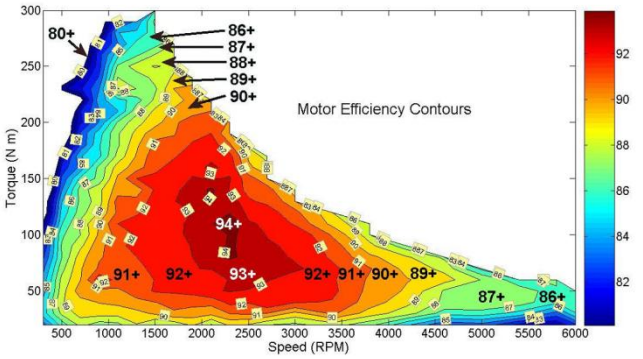

Figure 9: Measured Efficiency Map for 2004 Toyota Prius Motor [1]

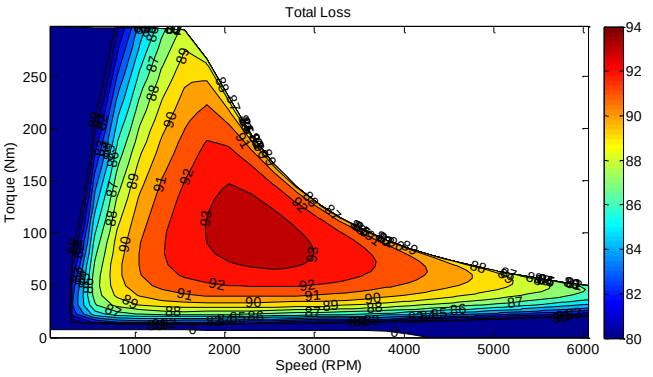

Figure 10: Computed Efficiency Map for 2004 Toyota Prius Motor

Computation Type	Time (Seconds)
Flux Linkage Model Calculation	54
Iron Loss Model Calculation	133
Optimal Is, γ and associated loss calculation at 450 operating points	17
Total	204

Table II: Computation time breakdown for generating the efficiency map shown in fig. 10

The mean magnitude of the error in prediction of the efficiency across 428 data points is 1% and the mean magnitude of the error in torque prediction is under 4%. The measured Prius data set is taken at a variety of temperatures with a stator winding temperature range of 50˚C-180˚C; this appears to be the source of most of the inaccuracies in torque and efficiency prediction.

5 Conclusions

To create an optimised BLAC PM motor design for an electric vehicle application analyses of the torque-speed capability and performance over the entire operational envelope are highly desirable. Current commercially available design tools do not provide means of accurately modelling the performance envelope of a BLAC PM motor with low enough computation time to be incorporated in an iterative design process. Through a combination of 2D finite element modelling and analytical models based around the established phasor diagram the performance envelope of a brushless AC PM motor can be modelled accurately and in a computationally efficient manner. The proposed technique computes a loss/efficiency map across the full torque speed envelope for a particular design in less than 4 minutes and is suitable for incorporation into a design process.

The proposed methods have been validated against experimental measurements taken from an in-house 35kW IPM traction motor design and from published data on the 2004 Toyota Prius motor. A good prediction of the maximum torque versus current operating envelope is obtained, as well as demonstrating the ability to accurately model the efficiency across the entire operational envelope.

Further work is planned that couples these techniques with thermal modelling enabling the generation of thermal maps to define the continuous and transient operating envelope of a particular design.

Acknowledgements

This work was supported by the Bristol University EPSRC funded Industrial Doctorate Centre in Systems (Grant EP/G037353/1) and Motor Design Ltd.

References

[1] C. W. Ayers, J. S. Hsu, L. D. Marlino, C. W. Miller, G. W. Ott, Jr., and C. B. Oland. Evaluation of 2004 Toyota Prius hybrid electric drive system interim report. Oak Ridge Nat. Lab., UT-Battelle, Oak Ridge, TN, ORNL/TM-2004/247, Nov. 2004

[2] N. Bianchi. *Electrical machine analysis using finite elements*. Power electronics and applications series. Taylor & Francis, 2005.

[3] J. S. Hsu, C. W. Ayers, C. L. Coomer, R. H. Wiles, "Report on Toyota/Prius Motor Torque Capability, Torque Property, No-Load Back EMF, and Mechanical Losses," Oak Ridge National Laboratory, Rep. ORNL/TM-2004/185, Sep. 2004

[4] P. H. Mellor, R. Wrobel, and D. Holliday. A computationally efficient iron loss model for brushless ac machines that caters for rated flux and field weakened operation. In *Proc. IEEE Int. Electric Machines and Drives Conf. IEMDC '09*, pages 490–494, 2009.

[5] M. Olaru, M.I. McGlip, T.J.E. Miller, PC-FEA 5.5, SPEED's Electrical Motors, SPEED Laboratory, University of Glasgow, 2010

[6] G. Qi, J. T. Chen, Z. Q. Zhu, D. Howe, L. B. Zhou, and C. L. Gu. Influence of skew and cross-coupling on flux-weakening performance of permanent-magnet brushless ac machines. 45(5):2110–2117, 2009.

[7] W. L. Soong and T. J. E. Miller. Field-weakening performance of brushless synchronous ac motor drives. *IEE Proceedings -Electric Power Applications*, 141(6):331–340, 1994.

Appendix

Flux Linkage Coefficient	d	q
$a_{d,q}$	0.07099	7.828e-005
$b_{d,q}$	0.0001857	3.893e-006
$c_{d,q}$	1.04e-005	0.0005459
$d_{d,q}$	7.616e-008	4.744e-007
$e_{d,q}$	3.258e-008	1.698e-008
$f_{d,q}$	1.762e-007	-1.271e-006
$g_{d,q}$	-2.832e-010	-7.963e-010
$h_{d,q}$	-1.702e-009	-4.466e-009
$j_{d,q}$	-1.555e-009	3.597e-010
$k_{d,q}$	2.148e-013	1.86e-012
$l_{d,q}$	3.254e-012	8.909e-012
$m_{d,q}$	2.832e-012	2.624e-012

Table III: Flux linkage coefficients for the 35kW IPM motor

Iron Loss Coefficient	Value
A_h	0.18063
A_e	0.00061697
B_h	0.13286
B_e	0.0015023

Table IV: Iron loss coefficients for the Toyota Prius Motor

Flux Linkage Coefficient	d	q
$a_{d,q}$	0.1572	0.0005329
$b_{d,q}$	0.002071	-3.565e-005
$c_{d,q}$	0.0002029	0.006977
$d_{d,q}$	-1.944e-006	3.435e-006
$e_{d,q}$	1.894e-006	-2.255e-007
$f_{d,q}$	-2.836e-006	-4.551e-005
$g_{d,q}$	-5.158e-009	-1.639e-008
$h_{d,q}$	-1.499e-008	-5.209e-008
$j_{d,q}$	5.204e-009	1.398e-007
$k_{d,q}$	5.098e-012	5.491e-011
$l_{d,q}$	4.187e-011	1.434e-010
$m_{d,q}$	2.541e-012	-1.52e-010

Table V: Flux linkage coefficients for the Toyota Prius motor